

# Long baseline LTS SQUID gradiometers with sub- $\mu\text{m}$ sized Josephson junctions

R Stolz<sup>1</sup> , M Schmelz<sup>1</sup> , S Anders<sup>1</sup>, J Kunert<sup>1</sup>, D Franke<sup>1</sup> and V Zakosarenko<sup>1,2</sup>

<sup>1</sup> Department Magnetometry, Leibniz Institute of Photonic Technology (Leibniz IPHT), Jena, Germany

<sup>2</sup> Supracon AG (SUP), Jena, Germany

E-mail: [ronny.stolz@leibniz-ipht.de](mailto:ronny.stolz@leibniz-ipht.de)

Received 9 October 2019, revised 13 February 2020

Accepted for publication 21 February 2020

Published 13 March 2020



## Abstract

In this paper, we present new integrated on-chip planar-type superconducting quantum interference device (SQUID) first order gradiometers, which are manufactured by a new *mix and match* fabrication technology combining sub- $\mu\text{m}$  sized Josephson junctions (JJs) with cm-scale pickup loops. The fabrication technology is described and the design is schematically shown. These sensors have high voltage swing and low flux noise and provide thus the best so far reported gradient resolution of about  $13\text{fT}/(\text{m} \cdot \sqrt{\text{Hz}})$ . These gradiometers were developed and implemented in instruments for applications in mineral exploration. They allow a better system dynamic range (ratio of maximal to minimal detectable signals) and a more effective use of the chip area. The gradiometer performance in terms of gradient resolution is compared against state of the art planar-type SQUID based gradiometers. Two models predicting a gradient noise limit as a function of the chip area and baseline of the gradiometer are discussed. The small geometric dimensions of the gradiometers are very important for future miniaturized instruments in mineral exploration. The comparison of our results with those models highlights the importance of a smaller JJs size for the reduction of the intrinsic gradiometer noise and geometrical dimensions.

Supplementary material for this article is available [online](#)

Keywords: SQUID, josephson junction, technology, magnetometry, gradiometer, sensitivity, high resolution

(Some figures may appear in colour only in the online journal)

## 1. Introduction

Magnetics is one of the most important and widely used geophysical methods which enables the detection of subtle spatiotemporal changes in the magnetic field amplitude and direction such as that of the Earth. With the improvements in magnetic field sensors (so called magnetometers), electronics, instrumentation, navigation, software and computers, this method is now deployed as a standard on a variety of platforms such as ground-based stationary and mobile, borehole, (sub-) marine, air- and spaceborne as well as on autonomous vehicles. Thus, it covers a wide range of spatial—from  $\mu\text{m}$  to global (and other planets/stars)—and temporal respectively frequency scales—from  $10^{-15}\text{Hz}$  for palaeomagnetic investigations to a few MHz [1]. This is the base for

a broad potential of applications [2, 3]. Improved planar-type gradiometers have beneficial features especially for biomagnetic measurements of neural responses [4] or (fetal) cardiac signals [5].

For this work the focus will be laid mainly on mineral exploration where magnetics is used to study the rock material properties in the Earth sub-surface. The historical development of the method is nicely summarized in [6]. There exists a broad variety of literature and reviews as well as case studies for magnetics used in mineral exploration which also covers instrumentation, data acquisition and processing as well as interpretation. Some useful examples for the interested reader are [7–9].

Magnetics as a potential field method, however, faces a significant pitfall: while the sensors have the potential to

measure sub-picoTesla magnetic field changes, the Earth magnetic field amplitude of typically between 20 and 65  $\mu\text{T}$ —depending on the measurement location and its spatio-temporal changes—is many orders of magnitude larger. Besides this, all vector-type magnetometer signals on movable platforms are overlaid by motion noise contributions up to a few hundred nanoTesla which exceed the potential resolution also by orders of magnitude. In the past, three solutions were presented: the use of (1) lower sensitive magnetometers such as fluxgates, (2) scalar-type magnetometers such as optically pumped magnetometers [10] measuring the total magnetic intensity<sup>3</sup>  $|\vec{B}|$  (TMI), and finally (3) magnetic gradiometers which measure spatial changes either of components of the magnetic induction  $\vec{B}$  or the TMI. The various gradiometer types are discussed in [11].

In this work we focus on the advancement of superconducting quantum interference device (SQUID) based intrinsic first-order planar-type gradiometers for mineral exploration which enable to reduce the influence of a homogeneous magnetic background field significantly to overcome the hurdles of using magnetometers in portable applications. An exhaustive overview on the variants and implications is provided in [12].

Various attempts have been made to develop partial or full tensor magnetic gradiometer (FTMG) instruments in the past, see [11], which measure either a single component or multiple components  $\partial B_i / \partial x_k$  with  $i, x_k \in (x, y, z)$  of the magnetic field gradient [13] up to the complete tensor:

$$\hat{B} = \begin{pmatrix} B_{xx} & B_{xy} & B_{xz} \\ B_{yx} & B_{yy} & B_{yz} \\ B_{zx} & B_{zy} & B_{zz} \end{pmatrix} \Rightarrow \begin{pmatrix} B_{xx} & B_{xy} & B_{xz} \\ B_{xy} & B_{yy} & B_{yz} \\ B_{xz} & B_{yz} & -B_{xx} - B_{yy} \end{pmatrix} \quad (1)$$

which reduces to five independent components according to Maxwell's equations for quasi-stationary conditions and in absence of flowing currents in the gradiometer's vicinity. This article builds on the earlier work on low temperature superconducting (LTS) SQUID based FTMG instruments using planar-type gradiometers [11, 14] commenced in 1997. The gradiometers used therein consist of two integrated on-chip superconducting pickup loops connected to the SQUID current sensor. The supercurrent flowing in the loops produces a magnetic flux in the SQUID  $\Phi_{SQ}$ . One of the main gradiometer characteristics is its effective area defined as the transfer function of the magnetic field  $B$  in one pickup loop to the flux in the SQUID  $A_{eff} = \Phi_{SQ} / B$  which leads to the effective volume  $V_{eff} = A_{eff} \cdot b$  measuring the magnetic field and the particular gradient tensor component as a function of its baseline  $b$ . Similarly the gradiometer response to the homogeneous field is a parasitic (magnetometer) area  $A_{par,i}$  with  $i \in (x, y, z)$ . The intrinsic suppression of a homogeneous magnetic field common mode rejection ratio (CMRR) of a first-order gradiometer is defined as

$C_{B,i} = A_{par,i} / V_{eff}$  with  $i \in (x, y, z)$  [11]. The used gradiometers on a 6 cm  $\times$  2 cm chip were fabricated in the standard 2.5  $\mu\text{m}$  Josephson junction technology [15] at Leibniz IPHT and provide baseline lengths of  $b = 3.5$  cm and intrinsic balance or CMRR of better than 5000. It can be improved to better than  $10^6$  using appropriate balancing procedures [12]. The reported noise-limited gradient field resolution was of the order of 60 fT/(m  $\cdot$   $\sqrt{\text{Hz}}$ ) with an onset frequency for the  $1/f$  noise of about 0.3 Hz [11].

At present there is a strong move towards miniaturized and unmanned airborne and sub-marine platforms for advanced magnetic field sensing instruments. In this context, the focus of this work is to develop improved first-order planar-type gradiometers with comparable or even lower intrinsic gradient field resolution and a higher voltage swing  $V_{PP}$  in combination with a significantly reduced geometrical size. Although the overall system resolution is mainly determined by motion noise at low frequencies<sup>4</sup> [16], new compensation algorithms [17] allow to reduce this disturbing contribution significantly. The noise limit by the signal-to-noise range of the digitizing unit [11] may be overcome in future e.g. by flux counting circuits [18–20].

A future topic is to combine the magnetic with electromagnetic (EM) methods in a joint instrument. Therein, very high resolving gradiometers will be used to detect EM signals of the Earth magnetic field or of active sources. For those methods the frequency range will extend from 10 Hz to about 100 kHz wherein the intrinsic noise of the gradiometers will play the major role in the instruments' resolution.

A first theoretical study on detecting EM signals with magnetic gradiometers was published by Sattel *et al* [21]. The estimated EM signal amplitude is so small that the current FTMG instruments e.g. [11] are not able to resolve it. Thus, a lower intrinsic noise of the gradiometers is required.

The higher voltage swing  $V_{PP}$  will result in an increased flux-to-voltage transfer  $V_\Phi$  and thereafter in a reduced overall SQUID and readout electronics noise as well as an increased system slew rate and thus improved stability [22] for the gradiometer in magnetically unshielded operation.

It has already been shown in e.g. [23] that an implementation of sub- $\mu\text{m}$  sized Josephson junctions (JJs) allows to reduce the intrinsic noise of the SQUID in conjunction with higher voltage swing. However, the lithographic tools can often not cover the required spatial dimensions ranging from sub- $\mu\text{m}$  up to about 5 cm for the large pickup loops. As one enabling solution for addressing this issue, we will introduce an advanced technology, called *mix and match*, which covers this range of dimensions for the improved gradiometers. In favor of fast turn-around times and costs we omitted the use of direct e-beam writing of the structures.

We will firstly report on the design of our advanced gradiometers in section two. The fabrication technology and

<sup>3</sup> Attempts to derive the TMI by vector-type sensors are challenging to implement since a calibration has to be done which takes care of non-orthogonality, scaling, and misalignment errors of the three orthogonal magnetometer signals, directional dependence of sensitivity of the magnetometers, nonlinearities caused by sensors and electronics, and cross talk.

<sup>4</sup> The investigated frequency range of the magnetic signal of geological sources depends of course on the platform speed, the geometrical dimensions of the source, the required spatial resolution and the distance of the sensor to the source. For airborne platforms at 30 m flight altitude or ground-based instruments the required frequency range may span from dc to  $f < 2$  Hz [17] or  $< 30$  Hz, respectively.

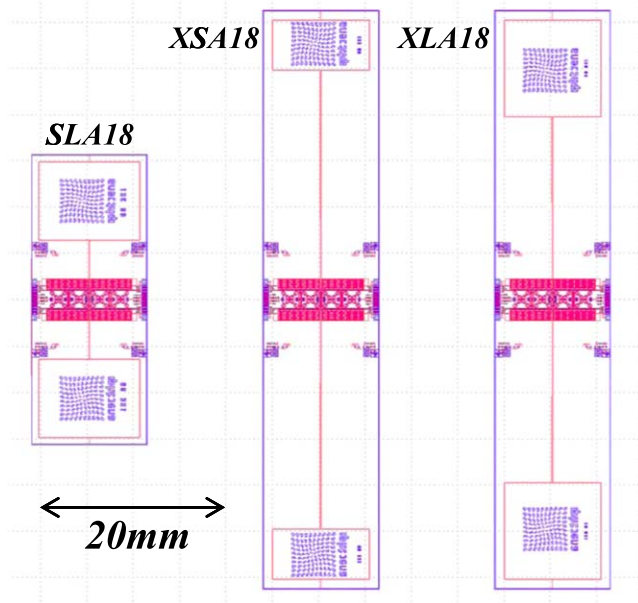


**Figure 1.** Newly developed gradiometer design variants XLA18, XSA18, and SLA18.

results of their characterization will be presented in the subsequent sections. Section five will provide an extensive literature study on planar-type gradiometers and models in order to compare and discuss the results of this work. From this comparison, conclusions will be drawn for possible future research topics on LTS (maybe also on high temperature superconducting (HTS)) SQUID based gradiometers.

## 2. Gradiometer designs

The four design variants of implementing thin film LTS SQUID based gradiometers (first-order and planar-type) are introduced e.g. in [24]. The gradiometric sensors in the present work were made as gradiometric pickup loops integrated on chip with Nb based SQUIDs. In order to couple the pickup loop inductance  $L_{AB}$  of a few nanoHenry to the SQUID inductance  $L_{SQ}$  with a few 100 pH an integrated input coil  $L_{EK}$  was used. The integrated input coil together with the pickup loop forms the so-called flux transformer.

In order to meet the demands for different applications, three pickup loop variants were designed: (1) large chip and large pickup loop size, (2), large chip and smaller pickup loops and (3) small chip size. The designs (1), (2), and (3) are called XLA18, XSA18, and SLA18, respectively. The design of the gradiometers is shown in figure 1 and the main parameters are summarized in table 1. To all pickup loop configurations the same clover-leaf structure SQUID was inductively coupled. The SQUID structure itself, a second order gradiometer which was first introduced in [15], was adapted only in the central region to implement the cross-type JJ technology. The modelled inductance of the SQUID and a single washer are about  $L_{SQ} = 368.6$  pH and  $L_W = 614$  pH [15], respectively. There are eight washers in the SQUID, two

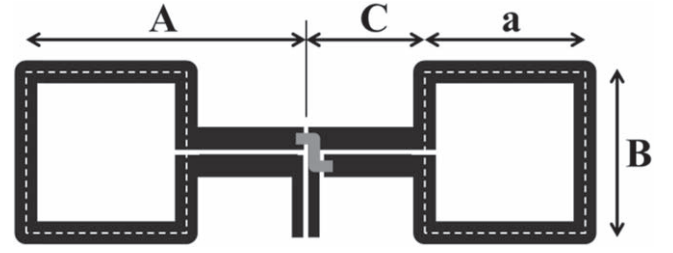


**Figure 2.** Sketch of a serial-type first-order gradiometer pickup loop which is inductively coupled to the SQUID.

**Table 1.** Modelled and measured parameters of the three gradiometer designs. The measured flux noise was about  $0.9 \mu\Phi_0/\sqrt{\text{Hz}}$  for all three types of gradiometers under investigation.

Variant	XLA18	XSA18	SLA18
Chip size (cm × cm)	6.25x1.25	6.25x1.25	3.125x1.25
Loop size (μm)			
<i>a</i>	10 440	5440	8455
<i>B</i>	10 440	10 440	10 940
<i>C</i>	19 780	24 780	6390
Baseline length <i>b</i> (cm)	5.0	5.5	2.1
Single loop inductance $L_A$ (nH)	57	45	47
Pickup loop inductance $L_{AB}$ (nH)	131.0	111.2	99.5
Modelled effective volume (mm <sup>3</sup> )	142.4	87.0	56.9
Mod. gradient noise (fT/(m · √Hz))	14.5	23.8	36.4
Measured effective volume (mm <sup>3</sup> )	142.8	90.0	59.1
Meas. white noise (fT/(m · √Hz))	13.0	20.7	31.5

connected as series gradiometer and four of those connected in parallel. Each washer hosts an input coupling coil for which the number of turns  $N_{EK}$  has to be chosen to gain the maximum effective volume. All separate input coils are connected in series to couple the flux in the pickup loops to the SQUID. The input coil is connected to the serial-type first-order gradiometer pickup loop, as shown in figure 2, with a baseline length of  $b = 2 \cdot C + a$ .

We will now give a short estimation for the gradiometer parameters based on our design: the inductance of one pickup loop  $L_A$  was modelled using FastHenry [25]. The results are listed in table 1. The inductance per unit length of a superconducting coplanar spoke, namely the inter-connection line between the two pickup loops (distance *C* in figure 2), can be approximated by [26]:

$$L_S' = \frac{\pi}{2} \cdot \frac{\mu_0}{\ln(4D_S/d_S)}. \quad (2)$$

Therein  $d_S$  and  $D_S = d_S + 2w_s$  are the spoke slit width and the total spoke width and  $w_s = 60 \mu\text{m}$  is the width of the superconducting wires of the spoke and the whole pickup loop. The total inductance of the spokes is  $L_S = 2L_S'C$ . For all three SQUID designs the dimensions of  $w_s = 60 \mu\text{m}$  and  $d_s = 5 \mu\text{m}$  are used resulting in an inductance per unit length

of about  $0.85 \text{ pH } \mu\text{m}^{-1}$ . The total inductance of the gradiometer pickup loop  $L_{AB}$  is therefore:

$$L_{AB} = 2L_A + L_S. \quad (3)$$

The gradiometer pickup loop circuit is inductively coupled to the SQUID with a total inductance  $L_{SQ}$ . The flux transfer is given by

$$T_\Phi = \frac{\Phi_{SQ}}{\Phi_A} = \frac{M_{EK}}{(L_{AB} + L_{EK})} = \frac{k\sqrt{L_{EK} \cdot L_{SQ}}}{(L_{AB} + L_{EK})} \quad (4)$$

with  $\Phi_A$  and  $\Phi_{SQ}$  being the magnetic fluxes in the pickup loop structure and in the SQUID.  $M_{EK}$  is the mutual inductance between the input coil and the SQUID. The input coil inductance to the SQUID  $L_{EK}$  is composed of the coupling inductance and a parasitic contribution mainly from the stripline inductance  $L_{ST}$ . For the used geometry an additional stripline inductance of about  $12.3 \text{ nH}$  [15] has to be taken into account. The optimization is done to maximize  $T_\Phi$  as a function of  $N_{EK}$ . Although the maximum of  $T_\Phi$  is found for  $N_{EK}$  between 5 and 6 for the XLA18 design, we have chosen a fixed  $N_{EK} = 6$  which may compensate further parasitic inductances to some extent. For the XSA18 and SLA18 a respective  $N_{EK}$  of 5 and 4 would be optimal. However, in order to reduce fabrication time and costs the same mask design with  $N_{EK} = 6$  was used which slightly reduces  $T_\Phi$  (below 5%) for the XSA18 and SLA18 design.

Finally, in any FTMG instrument the SQUID voltage noise is measured. It corresponds to an equivalent flux noise  $\Phi_N$  which is transformed into a gradient noise  $B_{ik,N}$  via the effective volume of the gradiometer  $V_{eff} = b \cdot A_{eff}$  [15] and thus for our gradiometers  $V_{eff} = a \cdot B(2C + a)T_\Phi$ .

Using all of these parameters, we estimated  $M_{EK} = 8.37 \text{ nH}$  and  $L_{EK} = 189.1 \text{ nH}$ . With these parameters the effective volume  $V_{eff}$  and a gradient noise for an expected equivalent flux noise of  $\Phi_N = 1 \mu\Phi_0/\sqrt{\text{Hz}}$  for the three gradiometer design were determined. The modelled values are listed in table 1.

### 3. Fabrication technology

The sensors were fabricated in the cross-type JJ technology described in [27] facilitating sub- $\mu\text{m}$  sized JJs with very low total junction capacitances  $C_0$  [27, 28]. This technology was adapted to a *mix and match* technique for the gradiometers' fabrication, as their large chip size is well beyond the i-line stepper's exposure field used for the definition of submicron JJs. In contrast to the fabrication discussed in [12], we firstly deposit a trilayer with (100 nm Nb, 14 nm Al/Al<sub>2</sub>O<sub>3</sub>, 60 nm Nb) by dc magnetron sputtering. The SQUID structures and alignment marks for the subsequent lithographic steps are exposed into the photoresist using an i-line stepper. We expose the same photoresist again with a mask aligner using these marks for the alignment of the structures. On the reticle for the mask aligner, the region of the SQUID is protected. Only the connecting wires for the gradiometer pickup loops remain open in order to connect with the according structures defined on the reticle for the mask aligner. The accuracy of

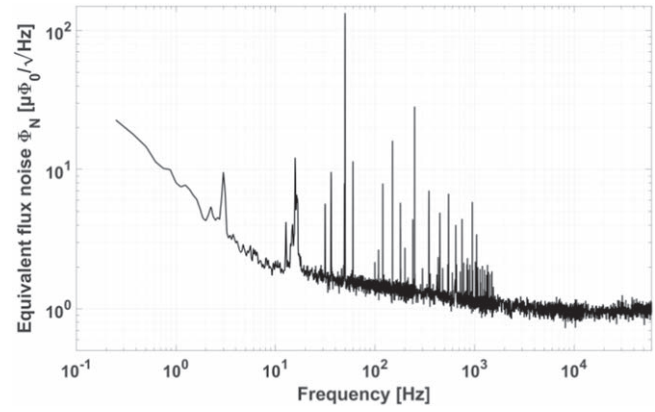


**Figure 3.** Representative example for the noise measurement of a gradiometer of XLA18 type.

overlap in this region between the two exposures needs to be better  $2 \mu\text{m}$ . If this overlap is not met, the resist is removed and these two exposures are repeated. After this lithographic step, the pickup loop and SQUID structure in the lower Nb wiring are finalized in parallel by reactive ion etching.

All subsequent fabrication steps correspond to the technology described in [27] for realization of  $0.8 \mu\text{m}$  side length JJs with a capacitance of  $C_0 = 40 \text{ fF}$ .

### 4. Gradiometer characterization

The gradiometers were characterized by standard four-point measurements in a dipstick immersed in liquid helium using a lead inside a Cryoperm™ shielding cylinder.

The values for the critical current, shunt resistance and voltage swing of the SQUIDs and the feedback coil coupling are typically in the range of  $I_C = 16.0 \mu\text{A}$ ,  $R_N = 9.2 \Omega$ ,  $V_{PP} = 110 - 120 \mu\text{V}$  and  $M_{FB}^{-1} = 9.5 \mu\text{A}/\Phi_0$ , respectively.

The noise characterization has been done with a directly coupled SQUID electronics [29] in a two-stage SQUID readout scheme [30] using a FFT spectrum analyzer of type HP35652B in order to determine the intrinsic equivalent flux noise of the gradiometers. From the measured voltage noise we derived the equivalent flux noise, as shown for example in figure 3, and finally the intrinsic gradient noise using the measured effective volume. The noise spectrum is characterized by a white noise floor for  $f > 5 \text{ kHz}$ , a slow increase of noise below this frequency, a strong rise with lowering the frequency below  $f = 10 \text{ Hz}$  and a number of discrete peaks. These features are caused by external disturbances (50 Hz and harmonics from the power supply network,  $16 \frac{2}{3} \text{ Hz}$  from the german railway, low frequency contributions by mechanical vibrations such as  $\approx 3 \text{ Hz}$  and  $\approx 32 \text{ Hz}$  etc) which are not completely suppressed due to a finite screening factor of the cryo-probe.

For the measurement of the effective volume  $V_{eff}$ , the according gradiometer was assembled in a non-magnetic plastic cryostat and operated using a directly coupled SQUID electronics. The cryostat was mounted in a four-wire planar gradient coil (a Maxwell coil set where each coil was split in



two halves of opposite magnetic field orientation, see Figure 1 in [31]) with dimensions of a 2.3 m side length cube. The current through the coil was precisely monitored with a temperature compensated series resistor.

Using the measured effective volume and flux noise, we calculated the equivalent gradient noise. The minimum white noise floor is  $13\text{fT}/(\text{m} \cdot \sqrt{\text{Hz}})$  for the XLA design which is the lowest value reported so far.

By considering table 1, one can observe that the modelled and measured values are in good agreement. The XLA18 structure has the optimal inductance match between SQUID and pickup loop for  $N_{EK} = 6$  and thus maximum  $T_\Phi$ . Further optimization of gradiometer performance in terms of  $T_\Phi$  especially for the type XSA18 and SLA18 by reducing  $N_{EK}$  to the optimal value in table 1 is possible. The impact of these changes will be discussed in the subsequent section.

## 5. Comparative study and discussion

In this section we will build on references and studies to compare and assess the quality of the results of this work against state-of-the-art gradiometers. Several studies have been performed so far in order to understand the characteristics and limitations of planar-type SQUID gradiometers of first order such as [32] and [15] for LTS or [33] for HTS implementations. Of course, this compilation of results is not comprehensive as many references do not give sufficient information either on gradient noise, effective volume, or on the used chip area for the planar-type gradiometer.

Within the context of gaining the minimum gradient noise and reduced geometrical dimensions of the gradiometers for miniaturized SQUID instruments, two models based on the used chip area  $A_{Chip}$  and on the gradiometer's baseline length  $b$  are hence of importance. Let us recap the according studies: drung discussed [32] the energy resolution  $\varepsilon$  of gradiometers as a function of the plasma frequency  $f_p$  as well as the gradient noise as a function of the chip area  $A_{Chip}$  and of a factor defined by the geometry of the pickup loop. For LTS implementations, he obtained a limitation for the spectral noise density depending on the used fabrication technology (see equation (3.11) in [32]):

$$\sqrt{S'_{Bo}} = 4 \cdot \sqrt{\varepsilon} \cdot g \quad [=B_{ik,N}]. \quad (5)$$

Therein,  $g$  is a geometrical factor of the gradiometer pickup loops as a function of the chip area

$$g \propto A_{Chip}^{-5/4} \quad (6)$$

for the optimum inductive coupling of  $L_{AB} = L_{EK}$ .

For a symmetric SQUID without inductively coupled gra-diometer pickup loop circuit and under optimum condition for the McCumber and screening parameter  $\beta_C = \beta_L = 1$  the minimum energy resolution was estimated to<sup>5</sup>

$$\varepsilon \approx 16k_B T \sqrt{L_{SQ} \cdot C_0}. \quad (7)$$

As a consequence, LTS fabrication technologies with low capacitive JJs such as the sub- $\mu\text{m}$  technology in this work are in favor and will provide very low gradient noise. Drung found a very good agreement between the performance of his digital SQUID gradiometer (Dr87 in figure 4) with the estimation in equation (5) for the used fabrication technology. It is represented by line A in figure 4 which corresponds to

$$K \cdot (A_{Chip}/\text{cm}^2)^{-5/4}. \quad (8)$$

As a result of this model, the gradient noise depends only on the fabrication technology, the SQUID inductance, and the according chip area. The SQUID parameters used in [32] are  $L_{SQ} = 51\text{pH}$  and  $C_0 = 0.38\text{pF}$  which results in a threshold (line A) of  $K = 252.9\text{fT}/(\text{m} \cdot \sqrt{\text{Hz}})$ . Please consider that the effective or also called 'screened' SQUID inductance  $L_{SQ,eff}$  has to be used in this calculation. It transforms the coupled SQUID inductance into the inductance of an uncoupled SQUID. More details and a formula on the effective SQUID inductance can be found in [36].

Figure 4 provides a comparison of the white floor of the gradient noise versus the chip area measured mostly in magnetically shielding. It does not take into account the low frequency noise as well as the effect of zero field cooled or field cooled operation of the planar-type gradiometers. For some of the references the chip dimensions were not listed and thus the gradiometer pickup loop circuit dimensions have been taken for estimating the required chip area.

The references *St95*–[37] and *St99a/b*–[15] are the predecessor development stages to this work on first-order planar-type gradiometers. The gradiometer design *St99b* was subsequently further optimized, mainly in the choice of the damping resistor in the input coil to the SQUID, which led to a lower noise floor of the so far unpublished variant *St15*. For the designs in this work, namely *SLA18*, *XSA18*, and *XLA18*, the dimensions of the pickup loop structure were changed and the design of the SQUID current sensor was only adapted to facilitate the new sub- $\mu\text{m}$  cross-type JJs. It is obvious that the sensor family *St95* and *St99a/b* lies above the threshold (line A in figure 4), since for those gradiometers the standard  $2.5\text{ }\mu\text{m}$  technology of Leibniz IPHT with a higher JJ capacitance  $C_0 = 0.69\text{pF}$  and a SQUID design with higher inductance [15] was used. The subsequent implementation of the sub- $\mu\text{m}$  JJ technology led to a significant decrease in the JJ capacitance and thus also to a much lower noise gradient floor and hence to a location of the *SLA18* and *XLA18* markers below the threshold (dashed line A) in figure 5.

Since the sensors of *Na87* and *We84* were magnetometers, Drung [32] transformed their magnetic field noise into gradient noise for comparison. The gradiometer named *Kn87* was also taken from [32].

The other LTS first-order planar-type SQUID gradiometer implementations were taken from the references: *Can91*–[38], *Can06*–[39], *Co79*–[40], *Du98a* and *Du98b*–[41], *DW82*–[42], *DW83*–[43], *Ei91a*–[44], *Gra09*–[45], *Ke78(a-c)*–[46], *Knu93*–[4], *Koy91*–[47], *Lee97*–[48],

<sup>5</sup> The minimum energy resolution according to [34, 35] is  $\varepsilon = 9k_B T L_{SQ}/R_0$ . For  $\beta_C = \beta_L = 1$  this formula can be written as  $\varepsilon \approx 16k_B T \sqrt{L_{SQ} \cdot C_0}$  which reasonably well predicts the behavior of LTS SQUIDs. Therein  $R_0$  is the shunt resistance of a single JJ.

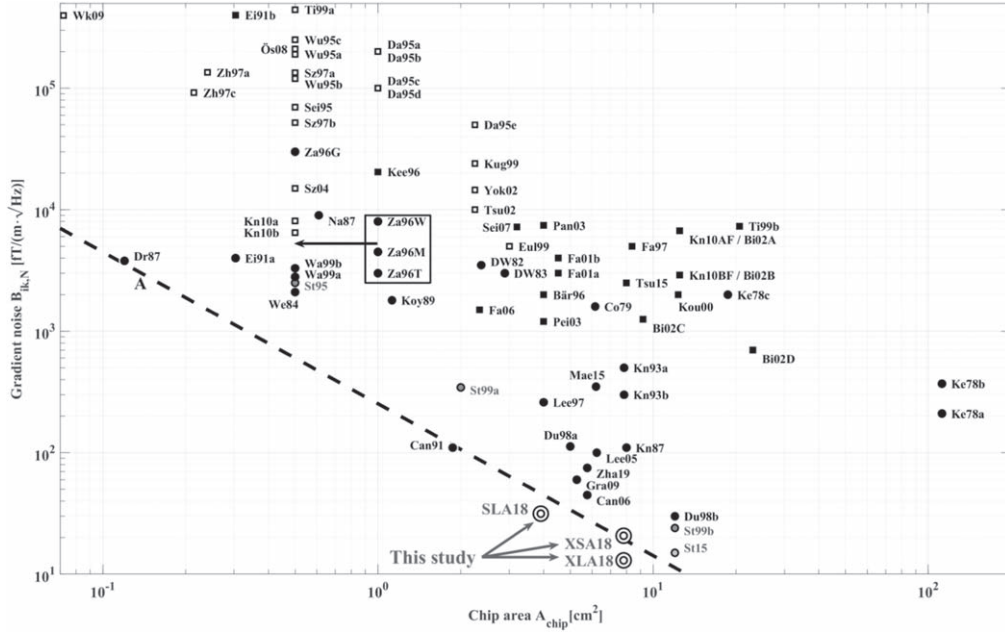


**Figure 4.** Comparative study of first-order planar-type LTS and HTS SQUID gradiometers with explanations in the text. The circles correspond to the LTS gradiometers while the filled and open squares relate to HTS SQUIDs with flip-chip (flux transformer) and single layer designs, respectively. The references are given as the first two or three letters from the first author and the year of publication (refer to text). Line A corresponds to the model derived by Drung in [32] which depends only on the fabrication technology, the SQUID inductance, and the chip area and corresponds very well to the according gradiometer (Dr87). The measured gradient noise of the SQUIDs developed in this work is marked by the double circles. It shows unprecedented performance in terms of noise in combination with small chip areas. Due to the sub- $\mu\text{m}$  JJs with low capacitance, the noise of the designs SLA18 and XLA18 is even below the threshold of line A.

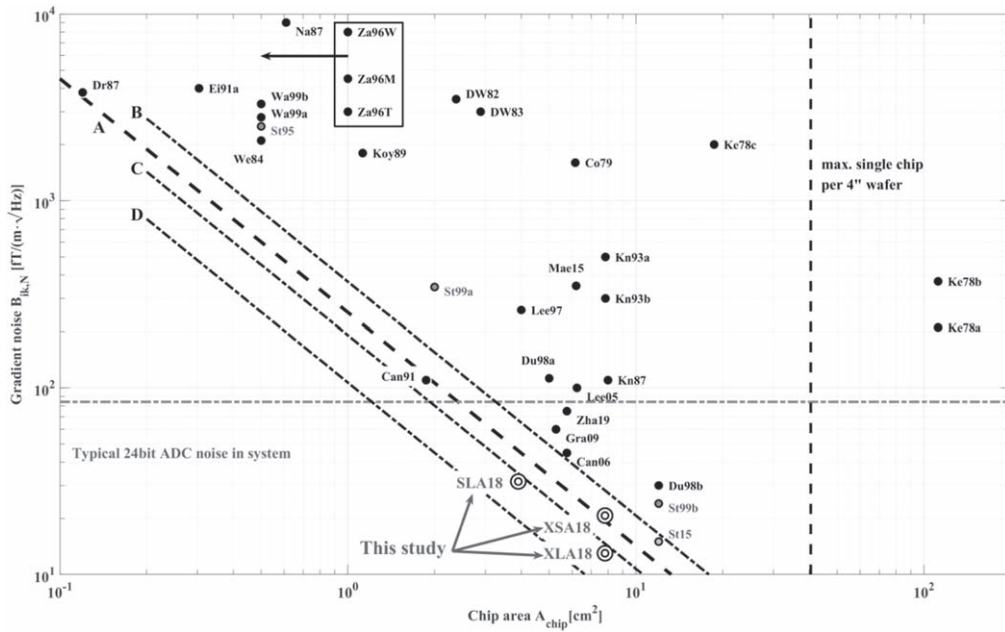


**Figure 5.** Comparative study of first-order planar-type LTS SQUID gradiometers. The lines A, B, C and D correspond to the model derived in [32] for various fabrication technologies which fit the experimental values for the according SQUIDs very well. The horizontal and vertical dashed lines represent the typical ADC noise limit and the maximum chip area for a 4 inch wafer, respectively.

*Lee05*–[49], *Mae15*–[50], *Wa99a* and *Wa99b*–[51], *Za96(G, M, T, W)*–[24] and *Zha19*–[52].

The according HTS implementations are marked with squares in figure 4. The single layer designs (open squares) correspond to: *Da(a-e)*–[53], *Eul99*–[54], *Kn10a* and

*Kn10b*–[55], *Kug99*–[56], *Ös08*–[57], *Sei95*–[58], *Sz97a* and *Sz97b*–[59], *Sz04*–[60], *Ti99a* and *Ti99b*–[61], *Tsu02*–[62], *Wk09*–[63], *Wu(a,b,c)*–[64], *Yok02*–[33], *Zha97a* and *Zha97c*–[65]. The flip-chip (flux transformer-type) variants are: *Bär96*–[66], *Bi02(A-D)*–[67], *Ei91b*–[44], *Fa97*–[68],

**Fa01a** and **Fa01b**–[69], **Fa06**–[70], **Kee96**–[71], **Kn10AF** and **Kn10BF**–[55], **Kou00**–[72], **Pan03**–[73], **Pei03**–[74], **Sei07**–[75], **Tsu15**–[76].

When considering the type of gradiometer, referred to [24], for  $A_{chip} < 3 \text{ cm}^2$  single layer designs were implemented such as washer or galvanometer SQUIDs. For larger areas galvanometer type SQUIDs are feasible, too. However, the flux transfer will decrease dramatically and an efficient use of the chip area is not possible. As a consequence, for  $A_{chip} > 3 \text{ cm}^2$  only fractional (equivalently multi-) loop or flux transformer designs were implemented. It should be considered that for increasing the baseline length  $b$  the parasitic inductance between the two pickup loops or the spokes inductance may deteriorate the gradiometers' performance in term of flux transfer again. Thus, for large chip areas mainly flux transformer type (mainly implemented in flip-chip configuration) designs are used. For an increasing chip area in figure 4 the HTS gradiometer performance gets worse compared to the LTS ones. For  $A_{chip} > 8 \text{ cm}^2$  a factor of fifty in gradient noise can be observed.

In figure 5 only LTS gradiometer implementations are depicted. Moreover, in this figure four threshold lines are now included:

- A. corresponds to the JJ technology used by Drung in [32],
- B. is the threshold for the  $2.5 \mu\text{m}$  technology at Leibniz IPHT with  $K = 368.5 \text{ fT}/(\text{m} \cdot \sqrt{\text{Hz}})$ ,
- C. the variant for the sub- $\mu\text{m}$  technology with  $0.8 \mu\text{m}$  JJs used for the variant **SLA18**, **XSA18**, and **XLA18** of gradiometers with  $K = 191.0 \text{ fT}/(\text{m} \cdot \sqrt{\text{Hz}})$  and
- D. the forecast for a technology with  $0.25 \mu\text{m}$  side length JJs which decreases  $K$  further down to  $106.7 \text{ fT}/(\text{m} \cdot \sqrt{\text{Hz}})$ .

**ST15** with the  $2.5 \mu\text{m}$  JJs fits well with the relating threshold B as well as **SLA18** and **XLA18** for the predicted threshold C of the accordingly used JJ technology and design. Their values are somewhat lower than the thresholds which points towards slightly lower effective SQUID inductances than assumed.

One can conclude from the comparison presented in figures 4 and 5 that the models based on [28] fit the LTS SQUID gradiometer sensitivities very well. They are thus suited to describe the gradient noise floor as a function of the chip area and the according technology of optimally coupled SQUIDs. In order to reduce the gradient noise in the future without changing the chip area, we have thus to decrease the JJ total capacitance and thus the JJ dimensions, e.g. such as down to  $0.25 \mu\text{m}$  side length, which itself will require significant efforts. This, however, will only result in a faint improvement in gradient resolution because equations (5) and (7) leading to  $B_{ik,N} \propto C_0^{1/4}$  and thus to a factor of 1.78 improved performance.

In figure 5 another threshold is given for the Leibniz IPHT technology: since only 4 inch wafers are used, a limit on the maximum usable chip area holds which is illustrated by the vertical dashed line at about  $A_{chip} = 40 \text{ cm}^2$ . Using this space for only one gradiometer per wafer might be problematic due to the finite yield of fully operational gradiometers per wafer. This was the reason to choose areas of about

$6 \times 2 \text{ cm}^2$  or  $6 \times 1 \text{ cm}^2$  for our gradiometers with highest gradient resolution.

Another, even more impeding, limit is illustrated by the gray dashed horizontal line at about an equivalent gradient noise floor of  $B_{ik,N} \approx 84.1 \text{ fT}/(\text{m} \cdot \sqrt{\text{Hz}})$  which corresponds to the input noise of the used 24 bit analogue to digital converters (ADCs). Let us roughly estimate: if an ADS1281<sup>TM</sup> made by Texas Instruments is used for digitization of the SQUID signal, its input voltage noise of about  $55 \text{ nV}/\sqrt{\text{Hz}}$  for an input voltage range of  $\pm 2.5 \text{ V}$  transforms via the feedback resistor of about  $1 \text{ k}\Omega$  with an inductive SQUID coupling of  $9.5 \mu\text{A}/\Phi_0$  to an equivalent flux noise of

$$S_{\Phi}^{1/2} \approx 55 \frac{\text{nV}}{\sqrt{\text{Hz}}} / \left[ 9.5 \frac{\mu\text{A}}{\Phi_0} \cdot 1 \text{ k}\Omega \right] = 5.8 \frac{\mu\Phi_0}{\sqrt{\text{Hz}}}. \quad (9)$$

A larger feedback resistance would decrease this limit but decrease the system dynamic range and hence worsen the system stability. An effective volume of about  $V_{\text{eff}} = 142.8 \text{ mm}^3$  for the **XLA18** gradiometer leads thus to the above stated equivalent gradient noise. As a consequence of this, the total system resolution is completely limited by the ADC. If the best gradient noise of the SQUIDs is required such as for the detection of EM signals, other readout schemes such as double SQUIDs or single SQUID electronics without reducing the dynamic range [77] like flux counting readout or dynamic field compensation etc have to be used. For that purpose the sub- $\mu\text{m}$  SQUIDs in this work are beneficial because of their large voltage swing.

Let us furthermore compare the effect of the baseline length on the intrinsic gradiometer noise. This second model was initially derived by Yokosawa *et al* [33] for HTS SQUIDs. Since their equivalent flux noise is often of the order of about  $\Phi_N = 10 \mu\Phi_0/\sqrt{\text{Hz}}$ , one may deduce a specification limit of the gradient noise depending on the inverse of the effective volume or the baseline length  $b$ . The latter dependence was extended in [33] to a relation of  $B_{ik,N} \sim b^{-2}$ . However, using the derivations from Drung [32], this relation will change to  $B_{ik,N} \sim b^{-2.5}$ . Due to the different dependences of the gradient noise on the baseline length, we compiled a diagram with the white gradient noise as a function of the baseline length of all the collected first-order planar-type SQUID gradiometers, see figure 6. Almost all single chip HTS as well as all washer-, galvanometer-, and multiloop-type LTS gradiometers can be found below a baseline length of about  $0.8 \text{ cm}$ . Above this baseline length all SQUIDs are of flux transformer type (for HTS made in flip-chip configuration).

Figure 6 also resumes the discussion of Yokosawa *et al* [33] which deduce from their data set that the flux noise of HTS SQUIDs has a lower limit and so does the white gradient noise floor. Their conclusion was a threshold of about

$$B_{ik,N} = 7 \text{ pT}/(\text{m} \cdot \sqrt{\text{Hz}}) \cdot [\text{cm}^2/b^2] \quad (10)$$

which corresponds to the black dashed line in figure 6. It is obvious from today's perspective that most of the HTS SQUID gradiometers lie above the threshold but also a significant number of them (well) below this threshold. Most of the LTS counterparts can also be observed below this

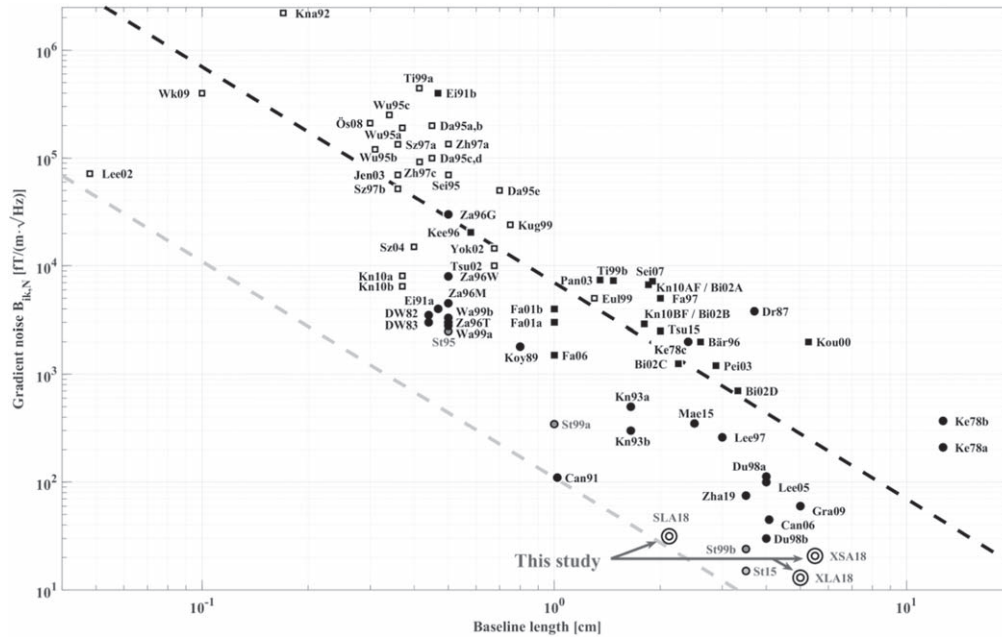


**Figure 6.** Comparative study of the white gradient noise versus the baseline length of the first-order planar-type SQUID gradiometers. The samples in this study are marked by double rings. The upper threshold was derived for HTS SQUIDs by Yokosawa *et al* [33] as a function of the inverse of the squared baseline length. Based on this model and the compiled data base from the literature, this work suggests a lower threshold for the LTS SQUIDs.

threshold. From our data collection, we suggest a parallel shift of the threshold to about

$$B_{ik,N} = 110 \text{fT}/(\text{m} \cdot \sqrt{\text{Hz}}) \cdot [\text{cm}^2/b^2]. \quad (11)$$

All planar-type gradiometers lay above this limit which is given by the gray dashed line in figure 6. It is obvious from this figure that the new gradiometers, presented in this work, used the available baseline length very efficient to provide very low gradient noise and even that the slightly longer base of the structure *XSA18* does not reduce the noise compared to the *XLA18* design.

Secondly, we derived a slope of  $B_{ik,N} \sim b^{-2.5}$  on the base of [32] which seem to fit the data in this work not well enough. This threshold is for clarity not shown in figure 6. Further investigation is required to clarify this dependence.

From figure 6 it is obvious that an increase of the baseline length results in a larger effective volume and thus in a reduced gradient noise. A future decrease of the SQUID flux noise, e.g. due to smaller JJ sizes and hence capacitances, would shift the threshold even further down.

## 6. Conclusion

In this work, we introduced a new family of first-order planar-type LTS SQUID gradiometers which implement sub- $\mu\text{m}$  JJs together with long baselines and large gradiometer effective volumes and thus provide the lowest so far measured gradient noise floor of down to  $13 \text{fT}/(\text{m} \cdot \sqrt{\text{Hz}})$ . The results agree well with the estimations. Moreover, two of the new SQUID designs leave further space for improvement by e.g. optimizing the number of input coil turns.

In the discussion section, two models for the gradient noise as a function of the geometry, namely the chip area and the baseline length, provide insights for the understanding of the characteristics and limitations of first-order planar-type SQUID gradiometers. A threshold on the gradient noise versus the inverse squared baseline is proposed. However, the dependence of the white gradient noise floor on the JJ capacitance and thus technology agrees very well with the measurement results and shows a way to improve the performance of the gradiometers in terms of noise by further shrinking the dimensions of the sub- $\mu\text{m}$  JJ without increasing the chip area. As a consequence, this work is a substantial step towards miniaturized SQUID instruments with small size gradiometers having lower gradient noise for the detection of very weak magnetic signatures such as proposed for electromagnetic methods.

## Acknowledgments

The authors acknowledge K Pippardt, M Sondermann, H Schneider for support with the thin film fabrication as well as the assembling and interconnection techniques.

This work was funded by the Federal Ministry of Education and Research under grant no. 033RU001B (AMTEG) in the framework of the ERA-NET Cofund on Raw Materials (ERA-MIN 2) funded under Horizon 2020.

## ORCID iDs

R Stolz <https://orcid.org/0000-0002-5629-4672>

M Schmelz <https://orcid.org/0000-0002-7911-0725>



## References

- [1] Constable C G and Constable S C 2013 Satellite magnetic field measurements: applications in studying the deep earth *The State of the Planet: Frontiers and Challenges in Geophysics* vol 150 (Washington DC: American Geophysical Union (AGU)) pp 147–59
- [2] Fagaly R L 2006 *Rev. Sci. Instrum.* **77** 101101
- [3] Anders S *et al* 2010 *Physica C* **470** 2079–126
- [4] Knuutila J E T, Ahonen A I, Hamalainen M S, Kajola M J, Laine P P, Lounasmaa O V, Parkkonen L T, Simola J T A and Tesche C D 1993 *IEEE Trans. Magn.* **29** 3315–20
- [5] Cuneo B F, Strasburger J F, Yu S, Horigome H, Hosono T, Kandori A and Wakai R T 2013 *Circulation* **128** 2183–91
- [6] Nabighian M N, Grauch V J S, Hansen R O, LaFehr T R, Li Y, Peirce J W, Phillips J D and Ruder M E 2005 *Geophysics* **70** 33ND–1ND
- [7] Hinze W J, Saad A H and Frese R von 2013 *Gravity and Magnetic Exploration: Principles, Practices, and Applications* (Cambridge: Cambridge University Press)
- [8] Nabighian M N and Asten M W 2002 *Geophysics* **67** 964–78
- [9] Vallée M A, Smith R S and Keating P 2011 *Geophysics* **76** W31–50
- [10] Grosz A, Haji-Sheikh M J and Mukhopadhyay S C 2017 *High Sensitivity Magnetometers* (Cham: Springer International Publishing)
- [11] Stolz R 2015 SQUIDS in Geophysics *Applied Superconductivity: Handbook on Devices and Applications* (Encyclopedia of Applied Physics) ed P Seidel (Weinheim: Wiley-VCH)
- [12] Vrba J 1996 SQUID gradiometers in Real environments // SQUID sensors: fundamentals, fabrication and applications *SQUID Sensors: Fundamentals, Fabrication and Applications* (NATO ASI series Series E, Applied Sciences) (Ed.), ed H Weinstock (Dordrecht: Springer Netherlands) pp 117–78
- [13] Linzen S, Chwala A, Schultze V, Schulz M, Schueler T, Stolz R, Bondarenko N and Meyer H G 2007 *IEEE Trans. Appl. Supercond.* **17** 750–5
- [14] Stolz R 2006 Supraleitende Quanteninterferenzdetektor-Gradiometer-Systeme für den geophysikalischen Einsatz *PhD Thesis* Friedrich-Schiller-University Jena Isle, Ilmenau
- [15] Stolz R, Fritzsche L and Meyer H G 1999 *Supercond. Sci. Technol.* **12** 806–8
- [16] Stolz R, Zakosarenko V, Schulz M, Chwala A, Fritzsche L, Meyer H G and Köstlin E O 2006 *Leading Edge* **25** 178–80
- [17] Schiffler M 2017 Processing, analysis and inversion of full tensor magnetic gradiometry data *PhD Thesis* Friedrich-Schiller-University Jena
- [18] McKay J, Vrba J, Betts K, Burbank M, Lee S, Mori K, Nonis D, Spear P and Uriel Y 1993 Implementation of a multi-channel biomagnetic measurement system using DSP technology *Proc. Canadian Conf. on Electrical and Computer Engineering Canadian Conf. on Electrical and Computer Engineering* (Vancouver, BC, Canada, 14–17 September 1993) (Piscataway, NJ: IEEE) pp 1090–3
- [19] Ludwig C, Kessler C, Steinfor A J and Ludwig W 2001 *IEEE Trans. Appl. Supercond.* **11** 1122–5
- [20] Zimmermann E *et al* 1997 HTS-SQUID Magnetometer with Digital Feedback Control for NDE Applications *Review of Progress in Quantitative Nondestructive Evaluation: Volume 16* ed D O Thompson and D E Chimenti (Boston, MA: Springer US) pp 2129–35
- [21] Sattel D and Macnae J 2001 *Geophys. Prospect.* **49** 309–20
- [22] Drung D 1996 Advanced SQUID read-out electronics *SQUID Sensors: Fundamentals, Fabrication and Applications* (NATO ASI Series Series E, Applied Sciences) (Ed.), ed H Weinstock (Dordrecht: Springer Netherlands) pp 63–116
- [23] Schmelz M, Stolz R, Zakosarenko V, Schoenau T, Anders S, Fritzsche L, Mueck M, Meyer M and Meyer H G 2012 *Physica C* **482** 27–32
- [24] Zakosarenko V, Warzemann L, Schambach J, Blüthner K, Berthel K-H, Kirsch G, Weber P and Stolz R 1996 *Supercond. Sci. Technol.* **9** A112–5
- [25] Kamon M, Tsuk M J and White J K 1994 *IEEE Trans. Microw. Theory Tech.* **42** 1750–8
- [26] Drung D, Knappe S and Koch H 1995 *J. Appl. Phys.* **77** 4088–98
- [27] Anders S, Schmelz M, Fritzsche L, Stolz R, Zakosarenko V, Schoenau T and Meyer H G 2009 *Supercond. Sci. Technol.* **22** 064012
- [28] Schmelz M, Stolz R, Zakosarenko V, Anders S, Fritzsche L, Schubert M and Meyer H G 2011 *Supercond. Sci. Technol.* **24** 015005
- [29] Oukhanski N, Stolz R and Meyer H G 2006 *Appl. Phys. Lett.* **89** 063502
- [30] Koshelets V P, Matlashov A N, Serpuchenko I L, Filippenko L V and Zhuravlev Y E 1989 *IEEE Trans. Magn.* **25** 1182–5
- [31] Tsuchiya D and Dohi T 2018 A compact magnetic resonance imaging system integrated micro RF and gradient coils for small sample measurement 2018 *IEEE Micro Electro Mechanical Systems (MEMS)* (Belfast, 21–25 January 2018) (Piscataway, NJ: IEEE) pp 426–9
- [32] Drung D 1987 Sensor und AD-Wandlerstufe auf einem Chip zur Präzisionsmessung von Magnetfeldgradienten mit Josephson-Kontakten *PhD Thesis* University of Karlsruhe
- [33] Yokosawa K, Tsukamoto A, Miyashita T, Kandori A, Suzuki D, Tsukada K and Takagi K 2002 *Supercond. Sci. Technol.* **15** 136–40
- [34] Tesche C D and Clarke J 1977 *J. Low Temp. Phys.* **29** 301–31
- [35] Bruines J J P, Waal V J de and Mooij J E 1982 *J. Low Temp. Phys.* **46** 383–6
- [36] Cantor R and Koelle D 2004 Practical DC SQUIDS: configuration and Performance *The SQUID Handbook* ed J Clarke and A I Braginski (Weinheim, FRG: Wiley-VCH Verlag GmbH & Co. KGaA) pp 171–217
- [37] Stolz R 1995 Integrierte planare Gradiometer-SQUID-Strukturen für den Einsatz in einer elektromagnetisch gestörten Umgebung *Diploma Thesis* Friedrich-Schiller-University Jena
- [38] Cantor R, Ryhänen T, Drung D, Koch H and Seppä H 1991 *IEEE Trans. Magn.* **27** 2927–31
- [39] Cantor R, Hall A and Matlachov A 2006 *J. Phys.: Conf. Ser.* **43** 1223–6
- [40] Cohen D 1979 Magnetic Measurement and Display of Current Generators in the Brain, Part I: The 2-D Detector 12th *International Conference on Medical and Biological Engineering* (Jerusalem) 15–16
- [41] van Duuren M J 1998 Advanced relaxation oscillation SQUIDS *PhD Thesis* Twente
- [42] Waal V J de and Klapwijk T M 1982 *Appl. Phys. Lett.* **41** 669–71
- [43] Waal V, de, van Nieuwenhuyzen G and Klapwijk T 1983 *IEEE Trans. Magn.* **19** 648–51
- [44] Eidelloth W, Oh B, Robertazzi R P, Gallagher W J and Koch R H 1991 *Appl. Phys. Lett.* **59** 3473–5
- [45] Granata C, Vettoliere A, Nappi C, Lisitskiy M and Russo M 2009 *Appl. Phys. Lett.* **95** 42502
- [46] Ketchen M B, Goubau W M, Clarke J and Donaldson G B 1978 *J. Appl. Phys.* **49** 4111–6
- [47] Koyanagi M, Kasai N, Chinone K, Nakanishi M, Kosaka S, Higuchi M and Kado H 1989 *IEEE Trans. Magn.* **25** 1166–9
- [48] Lee Y H, Kwon H C, Kim J M, Park Y K and Park J C 1997 *IEEE Trans. Appl. Supercond.* **7** 2752–5

- [49] Lee Y H 2005 *IEICE Trans. Electron.* **E88-C** 168–74
- [50] Maezawa M, Ying L, Gorwadkar S, Zhang G, Wang H, Kong X, Wang Z and Xie X 2015 *Phys. Proc.* **65** 173–6
- [51] Warzemann L 1999 Integrierte planare LTS-SQUID-Gradiometer für den Einsatz in gestörter Umgebung *PhD Thesis* Friedrich-Schiller-University Jena
- [52] Zhang X, Zhang G, Wang Y, Rong L, Zhang S, Wu J, Qiu L, Xie X and Wang Z 2019 *IEEE Trans. Appl. Supercond.* **29** 1–3
- [53] Daalmans G M, Bar L, Kuhl M, Uhl D, Selent M and Ramos J 1995 *IEEE Trans. Appl. Supercond.* **5** 3109–12
- [54] Eulenburg A, Romans E J, Carr C, Millar A J, Donaldson G B and Pegrum C M 1999 *Appl. Phys. Lett.* **75** 2301–3
- [55] Keenan S T, Young J A, Foley C P and Du J 2010 *Supercond. Sci. Technol.* **23** 25029
- [56] Kugai H, Nagaishi T, Hirano T and Itozaki H 1999 High Tc SQUID Gradiometer *Advances in Superconductivity XI: Proc. 11th Int. Symp. on Superconductivity (ISS '98) (Fukuoka, 16–19 November 1998)* ed N Koshizuka and S Tajima (Tokyo: s.l.: Springer Japan) pp 1213–6
- [57] Öisjöen F, Magnelind P, Kalabukhov A and Winkler D 2008 *Supercond. Sci. Technol.* **21** 34004
- [58] Seidel P, Zakosarenko V, Schmidl F, Dorrer L, Schneidewind H, Linzen S, Il'ichev E V and Darula M 1995 *IEEE Trans. Appl. Supercond.* **5** 2931–4
- [59] Schultze V, Stolz R, IJsselsteijn R, Zakosarenko V, Fritzsche L, Thrum F, Ilichev E and Meyer H G 1997 *IEEE Trans. Appl. Supercond.* **7** 3473–6
- [60] Schultze V, Drung D, IJsselsteijn R and Meyer H G 2004 *Supercond. Sci. Technol.* **17** S165–9
- [61] Tian Y J, Linzen S, Schmidl F, Dörner L, Weidl R and Seidel P 1999 *Appl. Phys. Lett.* **74** 1302–4
- [62] Tsukamoto A, Yokosawa K, Fukazawa T, Suzuki D, Tsukada K, Miyashita T, Kandori A and Takagi K 2002 *Physica C* **368** 41–4
- [63] Wakana H, Adachi S, Hata K, Hato T, Tarutani Y and Tanabe K 2009 *IEEE Trans. Appl. Supercond.* **19** 782–5
- [64] Wunderlich S, Schmidl F, Specht H, Dörner L, Schneidewind H, Hübner U and Seidel P 1998 *Supercond. Sci. Technol.* **11** 315–21
- [65] Zhang Y *et al* 1997 *IEEE Trans. Appl. Supercond.* **7** 2866–9
- [66] Bär L R, Daalmans G M, Barthel K H, Ferchland L, Kühnl M S M and Uhl D 1996 *Supercond. Sci. Technol.* **9** A87–91
- [67] Billings S 2002 *Superconducting Magnetic Tensor Gradiometer System for Detection of Underwater Military Munitions: SERDP Project MR-1661* (Ashland (USA): Sky Research, Inc.)
- [68] Faley M I *et al* 1997 *IEEE Trans. Appl. Supercond.* **7** 3702–5
- [69] Faley M I, Poppe U, Urban K, Paulson D N, Starr T N and Fagaly R L 2001 *IEEE Trans. Appl. Supercond.* **11** 1383–6
- [70] Faley M I, Poppe U, Urban K, Paulson D N and Fagaly R L 2006 *J. Phys.: Conf. Ser.* **43** 1199–202
- [71] Keene M N, Exon N J, Humphreys R G and Chew N G 1996 *J. Appl. Phys.* **79** 8783–91
- [72] Kouznetsov K A, Borgmann J and Clarke J 2000 *Rev. Sci. Instrum.* **71** 2873–81
- [73] Panaitov G I, Zhang Y, Krause H-J, Schubert J and Banzet M 2003 *IEEE Trans. Appl. Supercond.* **13** 841–4
- [74] Peiselt K, Schmidl F, Linzen S, Anton A S, Hübner U and Seidel P 2003 *Supercond. Sci. Technol.* **16** 1408–12
- [75] Seidel P, Becker C, Steppke A, Buettner M, Schneidewind H, Grosse V, Zieger G and Schmidl F 2007 *Supercond. Sci. Technol.* **20** S380–4
- [76] Tsukamoto A, Hato T, Adachi S, Motoori M, Sugisaki M and Tanabe K 2015 Development of magnetic prospecting system with HTS SQUID gradiometer for exploration of metal resources 2015 15th Int. Superconductive Electronics Conf. (ISEC) 2015 (Nagoya, Japan, 6–9 July 2015) (Piscataway, NJ: IEEE) pp 1–3
- [77] Drung D 2003 *Supercond. Sci. Technol.* **16** 1320–36